JOC The Journal of Organic Chemistry

Article

pubs.acs.org/joc

Mechanistic Study of Cp*Co^{III}/Rh^{III}-Catalyzed Directed C−H Functionalization with Diazo Compounds

Shuanglin Qu* and Christopher J. Cramer

Department of Chemistry, Chemical Theory Center, and Minnesota Supercomputing Institute, University of Minnesota, 207 Pleasant Street SE, Minneapolis, Minnesota 55455, United States

Supporting Information

ABSTRACT: Density functional theory calculations have been performed to provide mechanistic insight into a series of Cp*Co^{III}- and Cp*Rh^{III}-catalyzed directed C−H bond functionalizations with diazo-compound substrates. Co-based catalysis proceeds through five steps: C−H bond activation; C−C coupling via a concerted 1,2-aryl transfer; proto-demetalation; nucleophilic addition; and solvent-assisted methanol elimination. C−H bond activation is predicted to be reversible, consistent with deuterium-scrambling experiments. The higher Lewis acidity of Co compared to Rh for two otherwise identical catalysts increases the susceptibility of a coordinated carbonyl group to nucleophilic addition in the former, facilitating the formation of cyclized products not observed for Rh. Methanol elimination is predicted to be the turnover-limiting step for one substrate, and this is facilitated by solvent 2,2,2-trifluoroethanol (TFE) acting as a proton shuttle. Theory suggests that further tuning of acidity may offer opportunities for improving catalysis. We also assess the role of a pyridine group that leads to a different series of final steps in one Rh-based catalytic cycle, thereby enabling access to the otherwise suppressed cyclization product. Our study of an alternative Rh-based system having acetate ligands replaced with MeCN indicates that C−H bond activation is sensitive to those ligands and variation can affect which step is turnover-limiting.

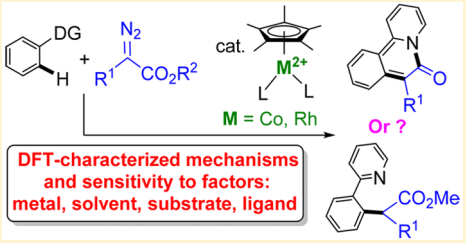

1. INTRODUCTION

In recent years, noble-metal-catalyzed directed C−H bond functionalization has been demonstrated to be a versatile approach in organic synthesis.[1−11] However, in the face of escalating costs and environmental concerns, efforts to replace these noble metals with earth-abundant first-row metals (e.g., cobalt) have been undertaken. Pioneered by the groups of Nakamura, Ackermann, and Yoshikai, inter alia, Co^{II}-catalyzed C−H activation has been used as an alternative for traditional noble-metal catalysts (Rh, Ru, and Pd) in various transformations.[12−14] Recently, a Cp*Co^{III} catalyst has been demonstrated to catalyze reactions for which a Cp*Rh^{III} catalyst has been previously demonstrated as competent by the groups of Ackermann, Ellman, and Glorius.[15−17] As first-row transition-metal-based catalytic systems often have unique reactivity that differs from noble-metal-based catalysts, there is also potential for such first-row systems to expand the scope of directed C−H functionalization.[18] For example, Kanai has demonstrated the unique reactivity of a Cp*Co^{III} catalyst toward directed C−H alkenylation/annulation compared to a related Cp*Rh^{III} catalyst.[19]

Carbene migratory insertion is well established as a possible method for directed C−H bond functionalization involving a reaction sequence of C−H metalation, metal−carbene formation, and migratory insertion.[20−22] As highly reactive carbene precursors, diazo compounds or *N*-tosylhydrazones have been employed as good coupling partners in C−H activations.[23−38] In 2011, Wang demonstrated a copper-catalyzed direct benzylation/allylation of 1,3-azoles with *N*-tosylhydrones,[25] and in 2012, Yu reported the Cp*Rh^{III}-catalyzed intermolecular cross-coupling of diazomalonates with arene C−H bonds.[26] Subsequent examples of diazo-involved C−H bond activation have been provided by the groups of Rovis,[27] Glorius,[28] Li,[30] Cui,[29] and Wang.[32,38] More recently, Glorius et al. developed a series of directed C−H bond functionalizations employing diazo compounds and catalyzed by Cp*Co^{III} or Cp*Rh^{III} catalysts.[18,39,40] Interestingly, the Cp*Co^{III} catalyst showed distinct reactivity compared to the congeneric Cp*Rh^{III} catalyst, with a cyclized product produced by the former and not the latter (Scheme 1, reactions I and II).[18,26] An analogous cyclized product *was* obtained with the Cp*Rh^{III} system, however, when the aromatic ring in the diazo substrate was taken to be a pyridine group instead of a phenyl (Scheme 1, reaction III).[39]

The mechanistic details rationalizing these variations in Cp*Co^{III}/Rh^{III}-catalyzed C−H bond functionalizations with diazo compounds have not yet been fully characterized, motivating our application of computational models to elucidate key factors affecting reactivity. In this work, we employ density functional theory (DFT) to compare the Cp*Co^{III} and Cp*Rh^{III} systems, focusing in part on the role of 2,2,2-trifluoroethanol (TFE) solvent in delivering cyclized products in the Cp*Co^{III} system[18] (TFE has been used as solvent in many recently reported Cp*Co/Rh^{III}-catalyzed reactions,[39−46] making this a topic of general relevance). We

Received: December 11, 2016
Published: December 22, 2016

DOI: 10.1021/acs.joc.6b02962
J. Org. Chem. 2017, 82, 1195−1204

Scheme 1. Directed C−H Bond Functionalizations with Diazo Compounds Catalyzed by Cp*Co^{III}/Rh^{III} Catalysts Reported by Glorius et al.[18,39]

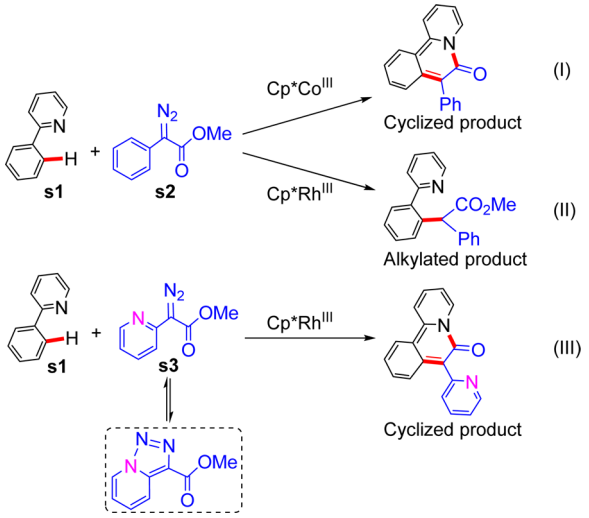

also assess the role of the pyridine group that results in a different series of final steps in the Rh-based catalytic cycle enabling access to the previously suppressed cyclization product. Our study of an alternative Rh-based system replacing acetate ligands with MeCN ligands shows that the C−H bond activation then requires assistance from the substrate itself, such that the turnover-limiting step of the whole catalytic transformation changes depending on acetate vs MeCN ligands.

2. COMPUTATIONAL METHODS

The Gaussian 09[47] suite of electronic structure programs was employed for all DFT calculations. With full atomistic representation, all structures were optimized in the gas phase at the M06-L[48−50]/BSI level, where BSI represents a basis set combination of SDD[51,52] for Rh and 6-31G(d,p)[53,54] for main group atoms and for Co. The local density functional M06-L accurately accounts for medium-range electron correlation effects like van der Waals interactions, and has been benchmarked to perform well in many studies of transition-metal-catalyzed chemistry.[48−50,55] Analytic harmonic vibrational frequencies were computed to verify the nature of all optimized stationary points as either minima or transition-state (TS) structures, having zero and one imaginary frequencies, respectively, and to compute thermal contributions to 298.15 K free energies. Improved energies were computed at M06-L/BSII single-point calculations including solvation effects with the SMD[56] continuum solvation model. Basis set BSII is a combination of SDD for Rh and def2-tzvpp[57−59] for all other atoms. Both SMD methanol and 2,2,2-trifluoroethanol computations were undertaken. Electronic energies in solution were converted to enthalpies and free energies at 298.15 K and 1 atm based on standard ideal-gas, rigid-rotator, harmonic-oscillator, particle-in-a-box thermodynamic partition functions. All frequencies below 50 cm^{-1} were replaced by 50 cm^{-1} when computing vibrational entropies.[60] Partial atomic charges were calculated at the M06-L/BSI level using the Natural Population Analysis (NPA) method which relies on localized Natural Bond Orbitals (NBOs).[61−63]

It has been observed that ideal-gas partition functions can sometimes lead to predicted entropies of activation for bimolecular reactions that are too negative,[64,65] owing in part, possibly, to the inaccuracy of employing a rotational partition function for a solute in solution rather than more appropriately accounting for the coupling of low-frequency solute modes with solvent librational motions, and the variations therein associated with combining reactive partners. Modeling such coupling requires detailed dynamics simulations with explicit (flexible) solvent, however, which is impractical at the DFT level. In the present study, we correct all solute free energies for the change in standard state concentration from 1 atm to 1 M (equal to RT ln(24.5), or 1.9 kcal/mol), while for solvents we correct further to account for their appropriate liquid concentrations at 298.15 K and 1 atm (13.3 and 24.8 M, respectively, for TFE and methanol, which require additional adjustments of RT ln(13.3) and RT ln(24.8), or 1.5 and 1.9 kcal/mol, respectively). Total energies and Cartesian coordinates for all structures are provided as Supporting Information.

3. RESULTS AND DISCUSSION

To model the overall reactions shown in Scheme 1, we considered first the catalytic cycle shown in Scheme 2, which is

Scheme 2. Possible Catalytic Cycle for Cp*M^{III}-Catalyzed Reactions Shown in Scheme 1

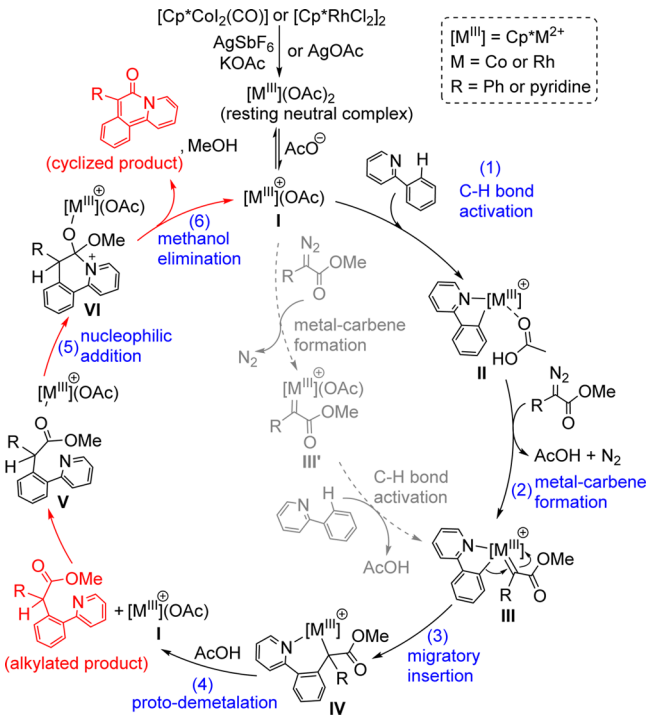

consistent with previous studies.[18,39,66] Preliminary halide abstraction from the Cp*M^{III} precatalyst ([Cp*Co(CO)I$_2$] or [Cp*RhCl$_2$]$_2$) by AgSbF$_6$/KOAc (or AgOAc) delivers a resting neutral complex [Cp*M^{III}(OAc)$_2$] that is saturated both coordinatively and electronically (i.e., it is an 18e^- complex). Previous studies have shown that the catalytically active species is the coordinatively unsaturated cationic complex **I**, in equilibrium with the resting neutral complex.[5,19,42,67,68] After formation of active catalyst **I**, the catalytic cycle proceeds through six steps: (1) C−H bond activation, (2) metal−carbene formation, (3) migratory insertion, (4) proto-demetalation, (5) nucleophilic addition, and (6) methanol elimination (reaction I). For the catalyst Cp*Rh^{III}(OAc)$_2$ (derived from [Cp*RhCl$_2$]$_2$ and AgSbF$_6$ + KOAc or AgOAc), when the R group in the diazo substrate is phenyl in the diazo substrate, alkylated product alone is obtained (reaction II),[18] i.e., from the standpoint of the organic substrate, in contrast to the Co case, the reaction stops after step 4. However, when the R group in the diazo substrate is pyridine, the organic component continues again through steps 5 and 6 to generate cyclized product (reaction III).[39] We examine the catalytic cycles associated with reactions I, II, and III in sections 3.1, 3.2, and

DOI: 10.1021/acs.joc.6b02962
J. Org. Chem. 2017, 82, 1195−1204

3.3, respectively. We also discuss in section 3.3 the catalysis of reaction III by $[Cp^*Rh(CH_3CN)_3](SbF_6)_2$,[39] which we find to proceed by a different mechanism.

3.1. Mechanism of Reaction I. Various spin states are available to $[Cp^*Co^{III}OAc]^+$ (**a1**) (derived from $[Cp^*CoI_2(CO)_2]$ and $AgSbF_6$/KOAc) and the several intermediates and TS structures associated with its catalytic activity. Computed energies for alternative spin states of several relevant Co^{III} species are provided in Table 1, and it is apparent that the singlet is the electronic ground state in every case, prompting us to restrict our evaluation of the overall reaction to the singlet surface. We further examined the relative energies of the triplet and singlet spin states for these Co^{III} species using other DFT functionals (in particular, M06, TPSS, and BP86). All functionals agree that the ground electronic state is the singlet in every case, although some variation in predicted state-energy splittings is observed across the various functionals (see Table S2).

Table 1. Relative Energies of Alternative Spin States for Selected Co^{III} Species[a]

Entry	Co^{III}-species	ΔE (kcal/mol)		
		S=0	S=1	S=2
1	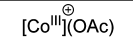	0.0	6.6	11.6
2	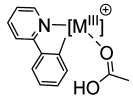	0.0	14.6	34.1
3	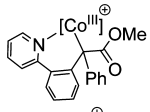	0.0	8.4	22.1
4	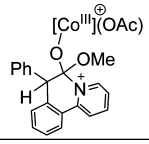	0.0	8.1	15.5

[a] $[Co^{III}]$ = Cp^*Co^{2+}. Optimizations of high spin states of cobalt–carbene species inevitably converge to the migratory insertion product, i.e., they are not stationary, and thus no energetic comparison is made in the table. Energies were calculated at the M06-L/BSII level.

C–H Bond Activation, Metal–Carbene Formation, and Migratory Insertion. A generally accepted mechanism for diazo-involved C–H bond functionalization begins with an initial C–H bond activation, followed by metal–carbene formation and migratory insertion.[18,20−40] Figure 1 shows a detailed mechanism for these three overall steps. Starting from the active catalyst $[Cp^*Co^{III}OAc]^+$ (**a1**), the 2-phenylpyridine (**s1**) coordinates to the Co center, leading to **a2**. In this latter structure, the pyridine N atom fills the vacant Co site, while a *meta*-C–H from the aryl group displaces one oxygen atom of the acetate group to form an agostic bond with the Co center that is hydrogen bonded to the displaced oxygen atom. The Co–C, Co–H, and O–H distances in **a2** are 2.328, 1.974, and 1.919 Å, respectively (see structure of **a2** in Figure 2). The agostic and hydrogen-bonding interactions weaken the C–H bond as judged by its elongation from 1.085 Å in **s1** to 1.116 Å in **a2**. C–H bond cleavage proceeds via TS structure **TSa1** with

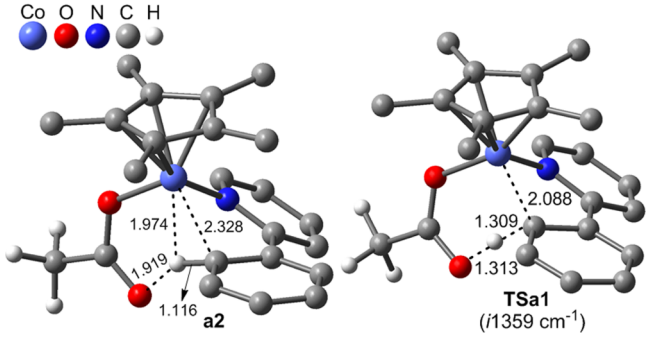

Figure 2. Selected bond lengths (Å) for optimized geometries of **a2** and **TSa1**. Hydrogen atoms other than that in flight are omitted for clarity. The imaginary frequency of **TSa1** is listed.

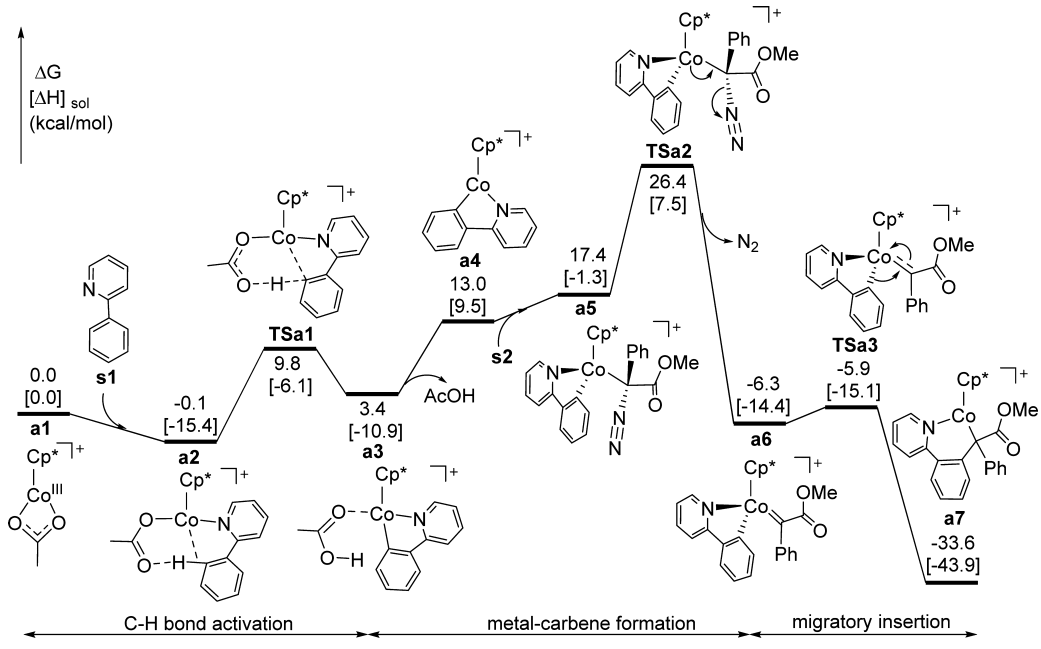

Figure 1. Free energy [enthalpy] profile (kcal/mol) for C–H bond activation, cobalt–carbene formation, and migratory insertion for reaction I.

DOI: 10.1021/acs.joc.6b02962
J. Org. Chem. 2017, 82, 1195−1204

a breaking C−H distance of 1.309 Å, and leads to cobaltacycle **a3**. The assisted C−H bond activation is consistent with a concerted metalation−deprotonation (CMD) mechanism as described by Fagnou,[69] and an ambiphilic metal−ligand activation (AMLA) mechanism as proposed by Davies and Macgregor.[70] Calculated energetics (ΔG_{rxn} = +3.5 kcal/mol, $\Delta G^{\ddagger}$ = 9.9 kcal/mol) indicate that the C−H bond activation should be reversible under experimental conditions, consistent with observed deuterium-scrambling experiments.[18] In addition, we examined an outer-sphere mechanism for C−H bond activation, but we found it to be less energetically favorable (see Figure S5).

Although currently accepted mechanisms for Cp*Co^{III}/Rh^{III} catalyzed directed C−H bond functionalizations assume that the first step is C−H bond activation,[18,20−40] in principle, the diazo substrate may alternatively react with the active catalyst **a1** to undergo metal−carbene formation as the first step (the gray pathway in Scheme 2). We compared the energetics of these two steps starting from **a1**. However, the coordination of **s2** to **a1** is predicted to be less favorable than the coordination of **s1** to **a1** by 11.7 kcal/mol (Figure S6), and the free energy of activation for metal−carbene formation is predicted to be 20.8 kcal/mol (**TSa1′**), which is above **TSa1** by 11.0 kcal/mol. The subsequent C−H bond activation step (**TSa2′**) along this pathway has an activation free energy of 33.7 kcal/mol (Figure S7), which is above that associated with **TSa2** by 7.3 kcal/mol. Thus, reaction of catalyst **a1** with **s1** will dominate at non-negligible concentrations of the latter.

Following C−H bond activation, acetic acid dissociates from **a3**, leaving a vacant coordination site in **a4** for subsequent metal−carbene formation. Coordination of diazo compound **s2** to the vacant Co site leads to **a5**. Subsequent N_2 extrusion proceeds through **TSa2** to give Co−carbene species **a6** with a free energy of activation of 26.4 kcal/mol relative to complexed educts. A following migratory insertion step proceeds almost without any free energy of activation (**TSa3** is higher in free energy than **a6** by only 0.4 kcal/mol), and results in cobaltacycle **a7**, which is predicted to be lower in free energy than initial separated reactants by 33.6 kcal/mol.

The C−C bond coupling process can proceed in a stepwise or concerted fashion (Scheme 3).[26] We find that both pathways are available in this instance (Figure 3). Concerted reaction proceeds from **a8**, which is a conformational isomer of **a5**

Scheme 3. Alternative Plausible Pathways for C−C Bond Coupling

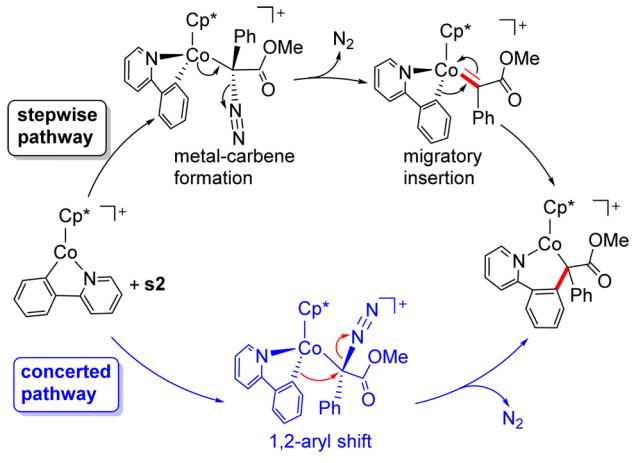

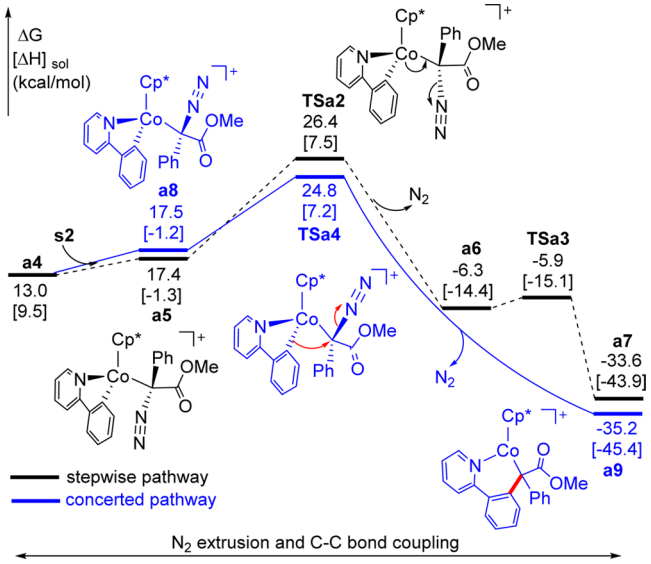

Figure 3. Free energy [enthalpy] profile (kcal/mol) for two plausible pathways of C−C bond formation for reaction I.

disposed to better facilitate backside displacement of N_2 in the 1,2-aryl shift TS structure **TSa4** (Figure 4, cf. **TSa2**) and

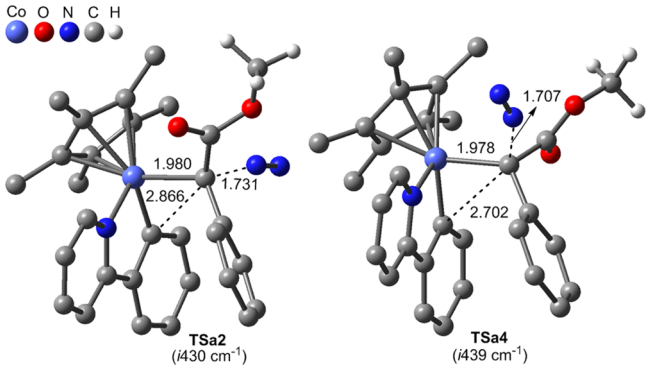

Figure 4. Selected bond lengths (Å) for optimized geometries of **TSa2** and **TSa4**. Most hydrogen atoms are omitted for clarity. Imaginary frequencies are also listed.

directly leads to the C−C coupling product **a9** (a conformational isomer of **a7**). We predict the concerted pathway to have a lower activation free energy than the stepwise path by 1.6 kcal/mol, which is within the error limits of our modeling protocol, suggesting that either or both paths may be operative experimentally.

Proto-Demetalation, Nucleophilic Attack, and Methanol Elimination. From C−C coupling product **a9**, proto-demetalation, nucleophilic attack, and methanol elimination proceed to deliver the final product and regenerate the active catalyst. Figure 5 details the energetics of these three steps; optimized geometries of key stationary points are provided in Figure 6. Proto-demetalation with acetic acid as the proton source proceeds through TS structure **TSa5** with a local free energy of activation of 28.8 kcal/mol, breaking the Co−C bond (which is stretched to 2.476 Å in the TS structure, Figure 6) and leading to the alkylated product **p1** and regenerated active catalyst **a1**.

To continue reacting, the carbonyl group of **p1** coordinates to Co in **a1**, giving **a10**. Subsequent nucleophilic addition of

DOI: 10.1021/acs.joc.6b02962
J. Org. Chem. 2017, 82, 1195−1204

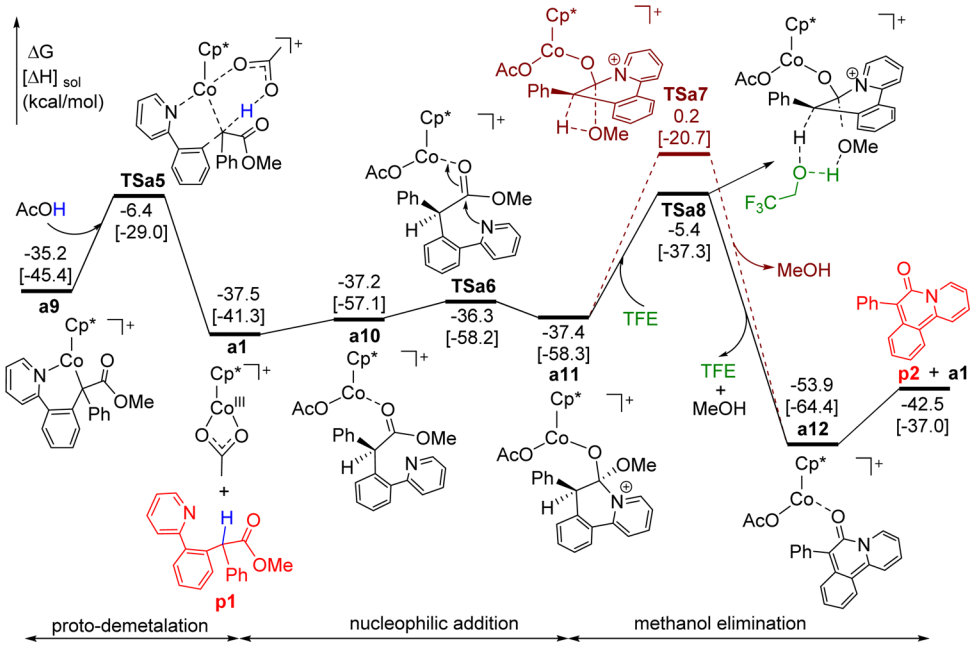

Figure 5. Free energy [enthalpy] profile (kcal/mol) for proto-demetalation, nucleophilic addition, and methanol elimination for reaction I.

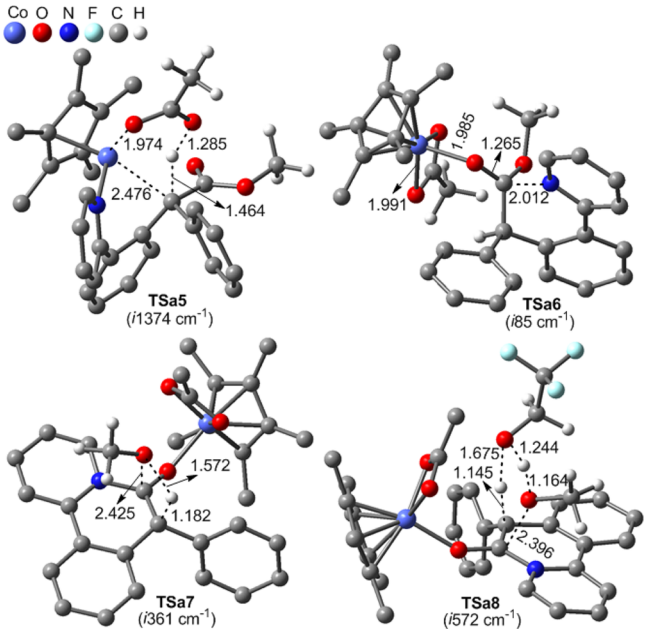

Figure 6. Selected bond lengths (Å) for optimized geometries of **TSa5−8**. Most hydrogen atoms are omitted for clarity. Imaginary frequencies are also listed.

pyridine to the activated carbonyl proceeds via transition state **TSa6**, leading to tetrahedral intermediate **a11**. The newly formed C−N bond in **a11** is weak, as judged by a bond length of 1.660 Å (vide infra), but it is maintained by the coordination of the oxide oxygen to the Co Lewis acid (if the Cp^*Co^{III} moiety is removed from **a11**, the organic structure reverts to **p1**).

After the nucleophilic addition step, loss of methanol is required to deliver the stable cyclized product **p2**, but direct 1,2-elimination from **a11** through **TSa7** is predicted to have a very high free energy of activation (37.7 kcal/mol). However, this activation free energy is reduced to 32.1 kcal/mol when a molecule of TFE solvent is recruited as a hydrogen-transfer (H-transfer)[71,72] catalyst (through **TSa8**). This is entirely consistent with the experimental observation[18] that solvent TFE is critical for this transformation. Methanol elimination drives aromatization, leading to **a12**, which can dissociate to cyclized product **p2** and **a1**, closing the catalytic cycle. The strong binding of **p2** to **a1** suggests that product inhibition can be a concern, and it may be that potassium cations present in solution from added KOAc assist in ion exchange to reduce such inhibition as concentrations of **p2** increase. Under such circumstances, the turnover-limiting step is TFE-assisted methanol loss, with its free energy of activation of 32.1 kcal/mol. At 393 K, transition-state theory predicts a reaction half-life of about 17 h for such an activation free energy, which is roughly consistent with the experimental conditions employed (80−120 °C, 12−24 h), especially if one considers that it may be that additional first-solvation-shell TFE molecules are recruited to further reduce the activation free energy slightly through further organization (however, given the complexity of considering such additionally microsolvated structures, and in particular their associated entropies, we did not explore this point further).

We examined the influence of the solvent acidity on the activation free energy for assisted methanol elimination. MeOH itself, which is less acidic than TFE, is less effective as a catalyst by 4.5 kcal/mol (see Figure S3) and would further disfavor formation of *product* MeOH if it were to be present as solvent. In principle, liberated AcOH could also act as a H-transfer shuttle, but its consumption in the proto-demetalation step keeps its concentration much too low to be competitive with solvent. However, as a stronger acid than TFE, it is worth considering buffering the reaction solution with AcOH (KOAc is already present). We compute that the free energy of activation for methanol elimination is reduced by 8.0 kcal/mol (see Figure S4) when using 1 M AcOH instead of solvent TFE as the proton shuttle. In addition to acting as the proton shuttle, the solvent TFE is also helpful in active species generation and maintaining a certain concentration of AcOH in

DOI: 10.1021/acs.joc.6b02962
J. Org. Chem. 2017, 82, 1195−1204

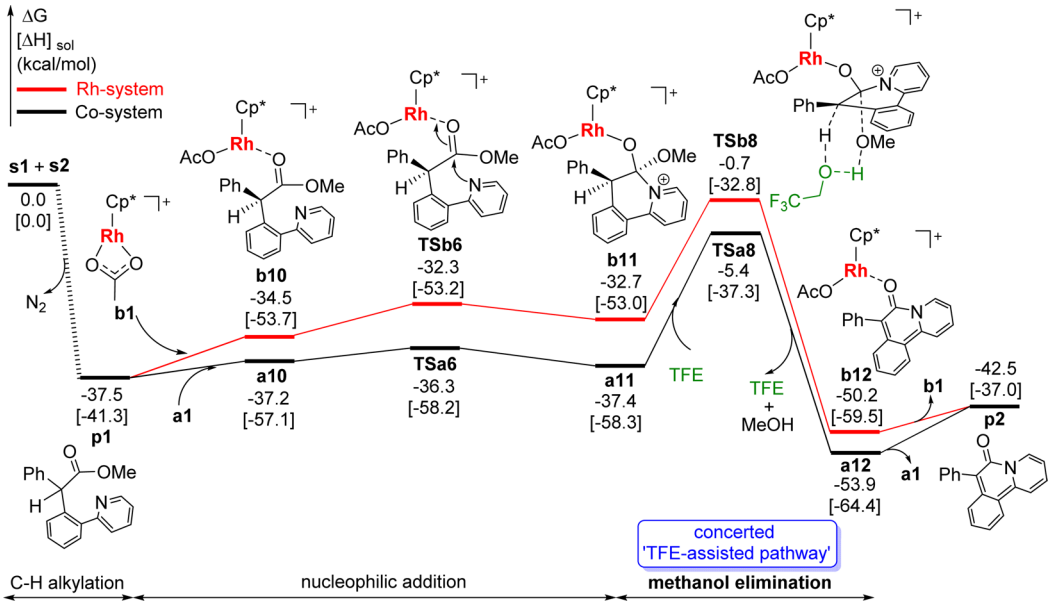

Figure 7. Free energy [enthalpy] profile (kcal/mol) comparing nucleophilic addition and methanol elimination for Cp*Co^{III} and Cp*Rh^{III} catalysts.

the system (which is critical for the proto-demetalation step); full details on the various roles of solvent TFE can be found in section 1 of the Supporting Information.

3.2. Comparisons of Cp*Co^{III} and Cp*Rh^{III} Systems. For the identical substrate as in reaction I, reaction II, which involves a Cp*Rh^{III} catalyst, leads to alkylated **p1** alone as the main product.[18,66] The mechanism for the formation of **p1** from **s1** + **s2** catalyzed by **b1** [Cp*Rh^{III}OAc]$^+$ (derived from $[Cp^*RhCl_2]_2$ and $AgSbF_6$+KOAc) is entirely analogous to that found for catalysis by **a1**: C−H bond activation is followed by metal−carbene formation, migratory insertion, and proto-demetalation (for full details see Figures S8 and S9). One difference for catalysis with **b1** is that no concerted 1,2-aryl transfer TS structure analogous to **TSa4** could be found: only stepwise C−C coupling was observed followed by migratory insertion with a very low barrier (Figure S9). The overall free energy of activation for generation of **p1** catalyzed by **b1** is predicted to be 26.0 kcal/mol (**TSb3** relative to separated reactants, Figure S9), which is very close to what is predicted for catalysis by **a1** (24.8 kcal/mol, **TSa4** relative to complexed educts). A question of more significant interest is why **b1** does not proceed further to deliver cyclized product **p2**.

Figure 7 compares free energies for transforming **p1** to **p2** catalyzed by **a1** and **b1**, respectively. Free energies of activation for nucleophilic addition are low for both catalysts: 1.2 kcal/mol for **TSa6** relative to **p1** + **a1** and 5.2 kcal/mol for **TSb6** relative to **p1** + **b1**, respectively. The C−N bonds resulting from nucleophilic addition are similarly weak, as supported by their long bond lengths (1.660 and 1.686 Å, respectively, Figure 8). It is apparent from computed Natural Population Analysis (NPA) partial atomic charges, however, that the Rh center is expected to be less Lewis acidic than the corresponding Co center: predicted charges are +0.421 and +0.943 for Rh and Co, respectively (Figure 8). Consistent with this analysis, the equilibrium between **b10** and **b11** is predicted to favor the former by 1.8 kcal/mol, while the equilibrium between **a10** and **a11** favors the latter by 0.2 kcal/mol. The lesser stabilization afforded by Rh complexation affects **TSb8** as well, leading to an overall free energy of activation for the cyclization process of 36.8 kcal/mol (**TSb8** vs **p1** + **b1**) compared to 32.1 (**TSa8** vs **p1** + **a1**). This additional activation free energy appears to render the cyclization too sluggish to be observed to a significant extent under the experimental conditions employed.

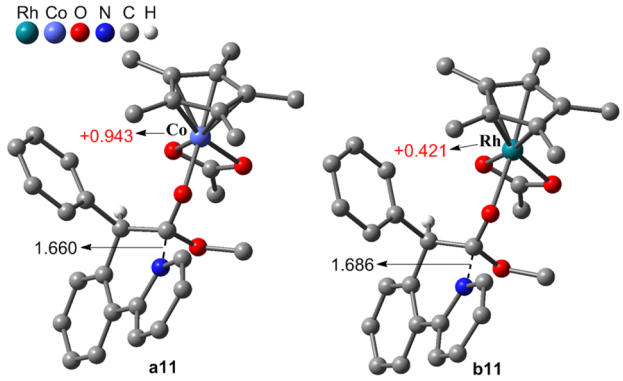

Figure 8. Selected bond lengths (black, Å) and atomic partial charges (red, au) for optimized geometries of **a11** and **b11**. Most hydrogen atoms are omitted for clarity.

3.3. Mechanism of Reaction III. Experiment indicates that the Cp*Rh^{III} catalyst *does* provide cyclized product when a pyridine group replaces a phenyl in the diazo substrate (reaction III, Scheme 1)[39] using either catalyst **b1** [Cp*Rh^{III}OAc]$^+$ (derived from $[Cp^*RhCl_2]_2$ + AgOAc) or **c1** $[Cp^*Rh(CH_3CN)_2]^{2+}$ (derived from $[Cp^*Rh(CH_3CN)_3](SbF_6)_2$) (see Table S1 in ref 9a). We first examine this mechanism for **b1**, and then contrast with **c1**.

The C−H activation, metal−carbene formation, migratory insertion, and proto-demetalation steps for reaction of **s1** + **s3** catalyzed by **b1** to generate **p3** are very similar to those for the reaction of **s1** + **s2** catalyzed by **b1** to generate **p1**, so we relegate details to the Supporting Information (see Figures S8 and S10). The free energy profile for cyclization of **s3** catalyzed by **b1** following formation of **p3** is shown in Figure 9. The bidentate coordination that can be achieved by **p3** owing to the pyridine group makes coordination of **p3** to **b1** to form **b13** exergonic by 4.7 kcal/mol (cf. formation of **b10**, which is endergonic by 3.0 kcal/mol, Figure 7). Interestingly, all efforts

DOI: 10.1021/acs.joc.6b02962
J. Org. Chem. 2017, 82, 1195−1204

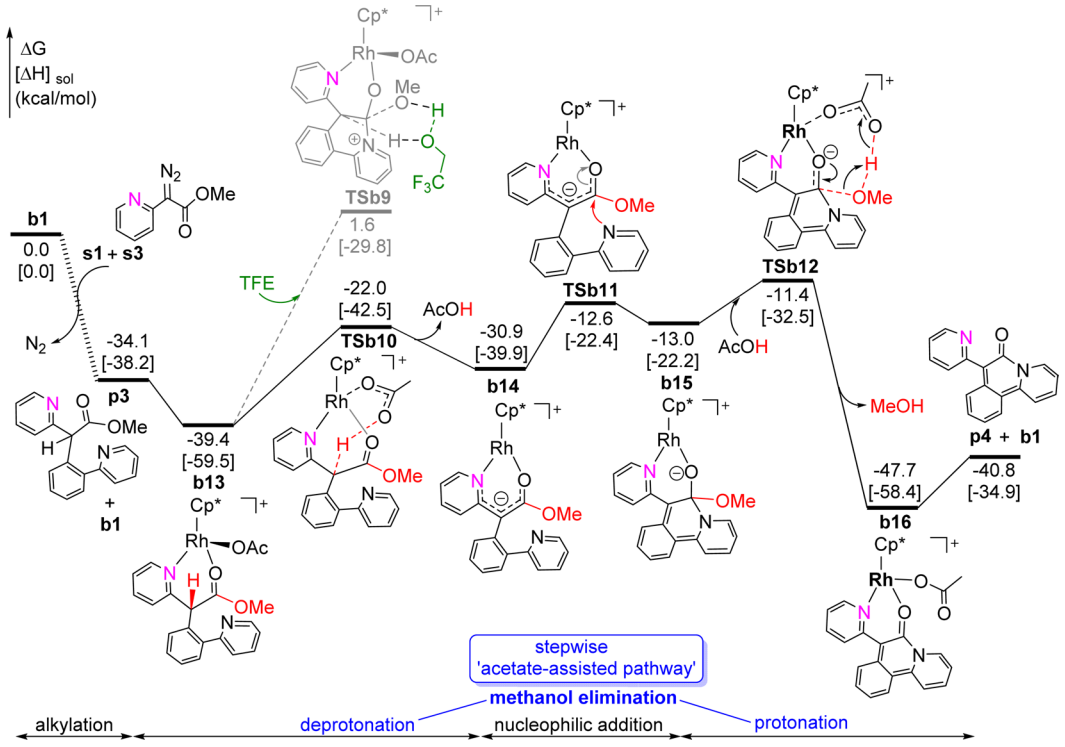

Figure 9. Free energy [enthalpy] profile (kcal/mol) for reaction III catalyzed by **b1**.

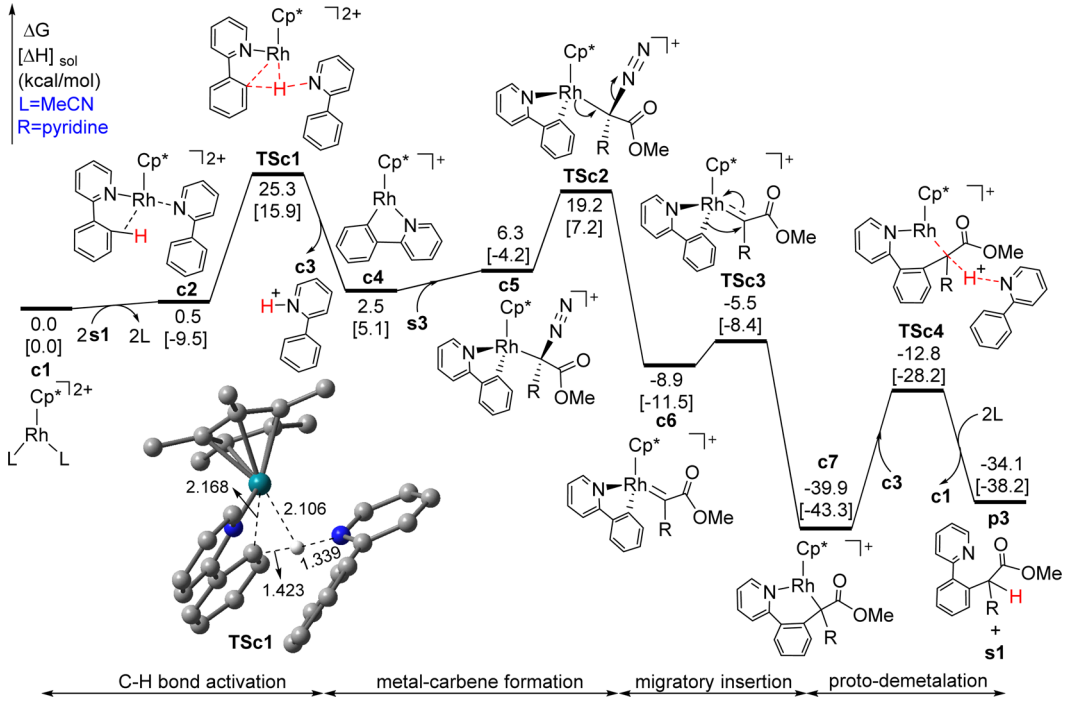

Figure 10. Free energy [enthalpy] profile (kcal/mol) for initial steps in reaction III catalyzed by **c1**.

to locate a TS structure for the nucleophilic addition of the free pyridine to the complexed carbonyl proved fruitless. Nor could an analogue to structure **b11** be found; no structure with even a weak C−N bond proved stationary. A concerted TS structure combining TFE assisted methanol elimination *with* C−N bond formation was found (**TSb9**), but with a very high free energy of activation of 41.0 kcal/mol relative to **b13** + TFE, this pathway is unlikely to be accessible under experimental conditions.

Instead, we found that coordination of the pyridine group to Rh substantially enhances the acidity of the benzylic proton, facilitating its abstraction by the acetate ligand with a free energy of activation of 17.4 kcal/mol (**TSb10** vs **b13**), leading to **b14**. From **b14**, nucleophilic attack and subsequent methanol elimination are predicted to take place with the overall process to generate **p4** having a free energy of activation of 28.0 kcal/mol (**TSb12** vs **b13**). This turnover-limiting activation free energy for **p4** is well below the 36.8 kcal/mol

DOI: 10.1021/acs.joc.6b02962
J. Org. Chem. 2017, 82, 1195−1204

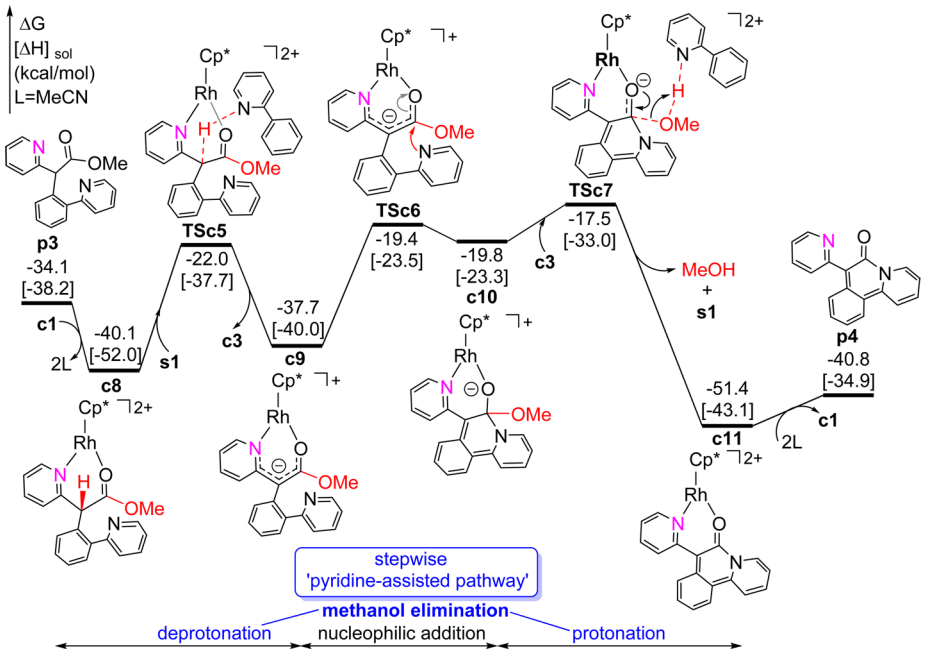

Figure 11. Free energy [enthalpy] profile (kcal/mol) for final steps in reaction III catalyzed by **c1** (**c9**, **TSc6**, and **c10** are the same structures as **b14**, **TSb11**, and **b15**, respectively).

predicted for **p2** catalyzed by **b1** (**TSb8** vs **p1** + **b1**, Figure 7), consistent with the failure to isolate cyclized product in the latter case. We note that the pyridine group (coordinated to the metal) is decisive in increasing the acidity of the benzylic proton. We investigated the analogous reaction paths for **s2** (without pyridine group), but free energies of activation in excess of 39.1 kcal/mol were found for either **a1** or **b1** as catalyst (see Figure S11), making this a noncompetitive route when R = phenyl in the diazo substrate.

It is noteworthy that cyclization of **s3** can also be catalyzed by $[Cp^*Rh(CH_3CN)_3](SbF_6)_2$, which lacks an acetate group.[39] Not unexpectedly, cyclization with this catalyst proceeds by a different mechanism. By analogy to the other reactions above, we start our computations from the unsaturated $16e^-$ cationic active species $[Cp^*Rh(CH_3CN)_2]^{2+}$ **c1** and explore the free energy profile for the first four steps to form alkylated product **p3** (see Figure 10). However, C−H bond activation in **s1** by **c1** is predicted to have a very high free energy of activation of 36.8 kcal/mol (see **TSc1′** in Figure S12), because the neutral MeCN ligand in **c1** is so much less basic than an anionic acetate ligand (SbF_6^- was not considered, but this ion is known to be an extremely weak and unlikely base[73,74]). Instead, the C−H bond activation is facilitated by the more basic pyridine group in the substrate **s1** via **TSc1** with an activation free energy of 25.3 kcal/mol, giving the protonated 2-phenylpridine **c3** and the rhodacycle **c4**. Calculated energetics (ΔG_{rxn} = +2.0 kcal/mol, $\Delta G^{\ddagger}$ = 25.3 kcal/mol) are consistent with the experimental observation that the C−H bond activation process can proceed readily under mild conditions.[39] The pyridine group in **s3** can also facilitate the C−H bond activation but is less effective than **s1** by 1.7 kcal/mol (see **TSc1″** in Figure S12), thus we only consider **s1** as a base for proton abstraction in the following. Similar to the other reactions above, metal−carbene formation and migratory insertion from **c4** proceeds readily via **TSc2** and **TSc3** to deliver more stable intermediate **c7**. Subsequently, proto-demetalation involving protonated **c3** occurs via **TSc4** with an activation free energy of 27.1 kcal/mol and delivers alkylated product **p3** as well as regenerated catalyst **c1** (after MeCN ligand recoordination).

The free energy profile for the remaining steps that generate cyclized product **p4** from **p3** with catalyst **c1** is shown in Figure 11. As for **b1** above, binding of **p3** in a bidentate fashion to **c1** is exergonic to deliver **c8**. By analogy to the pathway followed for **b1**, we examined the possibility of ligand-assisted deprotonation of the benzylic position in **c8**, but no transition state could be found for MeCN as a base and the deprotonation by MeCN is predicted to be endergonic by 29.8 kcal/mol. Again, the deprotonation by the more basic pyridine group in **s1** is more favorable with an activation free energy of only 17.9 kcal/mol (**TSc5**), leading to **c3** and **c9**. From **c9**, nucleophilic attack and subsequent methanol elimination by proton transfer from the protonated pyridine group in **c3** are predicted to take place to generate **p4** with a free energy of activation of 22.6 kcal/mol (**TSc7** vs **c8**). The overall methanol elimination process can be viewed as assisted by the pyridine group in **s1** in a stepwise fashion. Finally, dissociation of cyclized product **p4** and regeneration catalyst **c1** by MeCN ligand recoordination complete the catalytic cycle. The turnover-limiting step of reaction III catalyzed by **c1** is predicted to be the proto-demetalation step (**TSc4**, Figure 10) with a free energy of activation of 27.1 kcal/mol, which is 0.9 kcal/mol lower than that turnover-limiting step catalyzed by **b1** (28.0 kcal/mol, **TSb12** vs **b13**). This is consistent with the experimental study that catalyst **c1** is slightly more effective than **b1**.[39] Note that the turnover-limiting step of reaction III catalyzed by **c1** is different from that of the other reactions above (methanol elimination). Thus, while both catalysts **b1** and **c1** can promote reaction III to deliver the cyclized product, the turnover-limiting step of the catalytic transformation varies as a function of acetate vs MeCN ligands. Comparing reaction III with reactions I and II, the modification of the diazo substrate by replacing its phenyl ring with a pyridine ring substantially enhances acidity of the benzylic proton, which permits methanol elimination to proceed in a stepwise fashion assisted

DOI: 10.1021/acs.joc.6b02962
J. Org. Chem. 2017, 82, 1195−1204

by a ligand acetate (or the pyridine group in substrate **s1**) acting as a base.

4. CONCLUSIONS

We have exploited density functional theory to elucidate the mechanisms of various Cp*Co^{III}- and Cp*Rh^{III}-catalyzed directed C−H functionalizations with diazo compounds at the atomic level of detail. Co-catalysis proceeds through five steps: C−H bond activation (which precedes metal−carbene formation); C−C coupling via concerted 1,2-aryl transfer; proto-demetalation; nucleophilic addition; and solvent-assisted methanol elimination. C−H bond activation is predicted to be reversible, in agreement with deuterium-scrambling experiments.[18] The higher Lewis acidity of Co compared to Rh for otherwise identical catalysts increases the susceptibility of a coordinated carbonyl group to nucleophilic addition facilitating the formation of cyclized products not observed for Rh. Methanol elimination is the turnover-limiting step for one particular substrate, and this reaction is facilitated by solvent TFE that acts as a proton shuttle. In addition, the solvent TFE is also helpful for active species generation and maintaining a certain concentration of AcOH in the system. Thus, theory suggests that further tuning of the acidity of the reaction medium may offer opportunities for accelerating this reaction.

With a diazo substrate modified by the replacement of a phenyl ring with a pyridine ring, the previously suppressed cyclization product is accessed by Rh-based catalysis thanks to the substantially enhanced acidity of a benzylic proton when the pyridine unit coordinates to the metal. This results in a different series of final steps in the catalytic cycle with a ligand acetate (or the pyridine group of the substrate **s1**) acting as a base to abstract the benzylic proton, and subsequent nucleophilic cyclization. In an alternative Rh-based system replacing acetate ligands with MeCN ligands, the catalytic cycle again changes substantially, with the C−H bond activation assisted by the substrate itself and the turnover-limiting step being proto-demetalation rather than methanol elimination.

It is evident that a rich variety of mechanistic possibilities are associated with Cp*Co^{III}/Rh^{III}-catalyzed directed C−H functionalizations involving diazo compounds. Insights from theory into the sensitivity of individual elementary steps to such factors as metal, solvent, ligand basicity, and substrate-specific effects will be useful for the optimization of experimental conditions and further development in this area.

■ ASSOCIATED CONTENT

Supporting Information

The Supporting Information is available free of charge on the ACS Publications website at DOI: 10.1021/acs.joc.6b02962.

Discussions of the roles of the solvent TFE, additional calculated results, and energies and Cartesian coordinates (PDF)

■ AUTHOR INFORMATION

Corresponding Author

*E-mail: squ@umn.edu.

ORCID

Shuanglin Qu: 0000-0002-8122-9848

Christopher J. Cramer: 0000-0001-5048-1859

Notes

The authors declare no competing financial interest.

■ ACKNOWLEDGMENTS

We thank the NSF (CHE-1361595) and acknowledge the Minnesota Supercomputing Institute (MSI) at the University of Minnesota for providing resources that contributed to the research results reported within this paper.

■ REFERENCES

(1) Giri, R.; Shi, B.-F.; Engle, K. M.; Maugel, N.; Yu, J.-Q. *Chem. Soc. Rev.* **2009**, *38*, 3242−3272.
(2) Lyons, T. W.; Sanford, M. S. *Chem. Rev.* **2010**, *110*, 1147−1169.
(3) Satoh, T.; Miura, M. *Chem. - Eur. J.* **2010**, *16*, 11212−11222.
(4) Colby, D. A.; Bergman, R. G.; Ellman, J. A. *Chem. Rev.* **2010**, *110*, 624−655.
(5) Ackermann, L. *Chem. Rev.* **2011**, *111*, 1315−1345.
(6) Yeung, C. S.; Dong, V. M. *Chem. Rev.* **2011**, *111*, 1215−1292.
(7) Song, G.; Wang, F.; Li, X. *Chem. Soc. Rev.* **2012**, *41*, 3651−3678.
(8) Yamaguchi, J.; Yamaguchi, A. D.; Itami, K. *Angew. Chem., Int. Ed.* **2012**, *51*, 8960−9009.
(9) Wencel-Delord, J.; Glorius, F. *Nat. Chem.* **2013**, *5*, 369−375.
(10) Girard, S. A.; Knauber, T.; Li, C.-J. *Angew. Chem., Int. Ed.* **2014**, *53*, 74−100.
(11) Ackermann, L. *Acc. Chem. Res.* **2014**, *47*, 281−295.
(12) Chen, Q.; Ilies, L.; Nakamura, E. *J. Am. Chem. Soc.* **2011**, *133*, 428−429.
(13) Song, W.; Ackermann, L. *Angew. Chem., Int. Ed.* **2012**, *51*, 8251−8254.
(14) Gao, K.; Lee, P.-S.; Long, C.; Yoshikai, N. *Org. Lett.* **2012**, *14*, 4234−4237.
(15) Li, J.; Ackermann, L. *Angew. Chem., Int. Ed.* **2015**, *54*, 3635−3638.
(16) Yu, D.-G.; Gensch, T.; de Azambuja, F.; Vásquez-Céspedes, S.; Glorius, F. *J. Am. Chem. Soc.* **2014**, *136*, 17722−17725.
(17) Hummel, J. R.; Ellman, J. A. *J. Am. Chem. Soc.* **2015**, *137*, 490−498.
(18) Zhao, D.; Kim, J. H.; Stegemann, L.; Strassert, C. A.; Glorius, F. *Angew. Chem., Int. Ed.* **2015**, *54*, 4508−4511.
(19) Ikemoto, H.; Yoshino, T.; Sakata, K.; Matsunaga, S.; Kanai, M. *J. Am. Chem. Soc.* **2014**, *136*, 5424−5431.
(20) Davies, H. M. L.; Manning, J. R. *Nature* **2008**, *451*, 417−424.
(21) Xia, Y.; Zhang, Y.; Wang, J. *ACS Catal.* **2013**, *3*, 2586−2598.
(22) Hu, F.; Xia, Y.; Ma, C.; Zhang, Y.; Wang, J. *Chem. Commun.* **2015**, *51*, 7986−7995.
(23) Fulton, J. R.; Aggarwal, V. K.; de Vicente, J. *Eur. J. Org. Chem.* **2005**, *2005*, 1479−1492.
(24) Zhang, Y.; Wang, J. *Chem. Commun.* **2009**, 5350−5361.
(25) Zhao, X.; Wu, G.; Zhang, Y.; Wang, J. *J. Am. Chem. Soc.* **2011**, *133*, 3296−3299.
(26) Chan, W.-W.; Lo, S.-F.; Zhou, Z.; Yu, W.-Y. *J. Am. Chem. Soc.* **2012**, *134*, 13565−13568.
(27) Hyster, T. K.; Ruhl, K. E.; Rovis, T. *J. Am. Chem. Soc.* **2013**, *135*, 5364−5367.
(28) Shi, Z.; Koester, D. C.; Boultadakis-Arapinis, M.; Glorius, F. *J. Am. Chem. Soc.* **2013**, *135*, 12204−12207.
(29) Cui, S.; Zhang, Y.; Wang, D.; Wu, Q. *Chem. Sci.* **2013**, *4*, 3912−3916.
(30) Yu, X.; Yu, S.; Xiao, J.; Wan, B.; Li, X. *J. Org. Chem.* **2013**, *78*, 5444−5452.
(31) Ai, W.; Yang, X.; Wu, Y.; Wang, X.; Li, Y.; Yang, Y.; Zhou, B. *Chem. - Eur. J.* **2014**, *20*, 17653−17657.
(32) Hu, F.; Xia, Y.; Ye, F.; Liu, Z.; Ma, C.; Zhang, Y.; Wang, J. *Angew. Chem., Int. Ed.* **2014**, *53*, 1364−1367.
(33) Jeong, J.; Patel, P.; Hwang, H.; Chang, S. *Org. Lett.* **2014**, *16*, 4598−4601.
(34) Liang, Y.; Yu, K.; Li, B.; Xu, S.; Song, H.; Wang, B. *Chem. Commun.* **2014**, *50*, 6130−6133.
(35) Ye, B.; Cramer, N. *Angew. Chem., Int. Ed.* **2014**, *53*, 7896−7899.
(36) Li, X. G.; Sun, M.; Liu, K.; Jin, Q.; Liu, P. N. *Chem. Commun.* **2015**, *51*, 2380−2383.

DOI: 10.1021/acs.joc.6b02962
J. Org. Chem. 2017, 82, 1195−1204

(37) Shi, J.; Zhou, J.; Yan, Y.; Jia, J.; Liu, X.; Song, H.; Xu, H. E.; Yi, W. *Chem. Commun.* **2015**, *51*, 668−671.
(38) Xia, Y.; Liu, Z.; Feng, S.; Zhang, Y.; Wang, J. *J. Org. Chem.* **2015**, *80*, 223−236.
(39) Kim, J. H.; Gensch, T.; Zhao, D.; Stegemann, L.; Strassert, C. A.; Glorius, F. *Angew. Chem., Int. Ed.* **2015**, *54*, 10975−10979.
(40) Kim, J. H.; Greßies, S.; Glorius, F. *Angew. Chem., Int. Ed.* **2016**, *55*, 5577−5581.
(41) Gensch, T.; Vasquez-Cespedes, S.; Yu, D. G.; Glorius, F. *Org. Lett.* **2015**, *17*, 3714−3717.
(42) Bunno, Y.; Murakami, N.; Suzuki, Y.; Kanai, M.; Yoshino, T.; Matsunaga, S. *Org. Lett.* **2016**, *18*, 2216−2219.
(43) Sen, M.; Emayavaramban, B.; Barsu, N.; Premkumar, J. R.; Sundararaju, B. *ACS Catal.* **2016**, *6*, 2792−2796.
(44) Grigorjeva, L.; Daugulis, O. *Org. Lett.* **2014**, *16*, 4688−4690.
(45) Berkessel, A.; Krämer, J.; Mummy, F.; Neudörfl, J. M.; Haag, R. *Angew. Chem., Int. Ed.* **2013**, *52*, 739−743.
(46) Shuklov, I. A.; Dubrovina, N. V.; Boerner, A. *Synthesis* **2007**, *2007*, 2925−2943.
(47) Frisch, M. J.; Trucks, G. W.; Schlegel, H. B.; Scuseria, G. E.; Robb, M. A.; Cheeseman, J. R.; Scalmani, G.; Barone, V.; Mennucci, B.; Petersson, G. A.; Nakatsuji, H.; Caricato, M.; Li, X.; Hratchian, H. P.; Izmaylov, A. F.; Bloino, J.; Zheng, G.; Sonnenberg, J. L.; Hada, M.; Ehara, M.; Toyota, K.; Fukuda, R.; Hasegawa, J.; Ishida, M.; Nakajima, T.; Honda, Y.; Kitao, O.; Nakai, H.; Vreven, T.; Montgomery, J. A., Jr.; Peralta, J. E.; Ogliaro, F.; Bearpark, M.; Heyd, J. J.; Brothers, E.; Kudin, K. N.; Staroverov, V. N.; Kobayashi, R.; Normand, J.; Raghavachari, K.; Rendell, A.; Burant, J. C.; Iyengar, S. S.; Tomasi, J.; Cossi, M.; Rega, N.; Millam, J. M.; Klene, M.; Knox, J. E.; Cross, J. B.; Bakken, V.; Adamo, C.; Jaramillo, J.; Gomperts, R.; Stratmann, R. E.; Yazyev, O.; Austin, A. J.; Cammi, R.; Pomelli, C.; Ochterski, J. W.; Martin, R. L.; Morokuma, K.; Zakrzewski, V. G.; Voth, G. A.; Salvador, P.; Dannenberg, J. J.; Dapprich, S.; Daniels, A. D.; Farkas, O.; Foresman, J. B.; Ortiz, J. V.; Cioslowski, J.; Fox, D. J. *Gaussian 09*, Revision A.01; Gaussian, Inc.: Wallingford, CT, 2009.
(48) Zhao, Y.; Truhlar, D. G. *Acc. Chem. Res.* **2008**, *41*, 157−167.
(49) Zhao, Y.; Truhlar, D. *Theor. Chem. Acc.* **2008**, *120*, 215−241.
(50) Zhao, Y.; Truhlar, D. G. *J. Chem. Phys.* **2006**, *125*, 194101.
(51) Andrae, D.; Haussermann, U.; Dolg, M.; Stoll, H.; Preuss, H. *Theor. Chem. Acc.* **1990**, *77*, 123−141.
(52) Roy, L. E.; Hay, P. J.; Martin, R. L. *J. Chem. Theory Comput.* **2008**, *4*, 1029−1031.
(53) Hehre, W. J.; Ditchfield, R.; Pople, J. A. *J. Chem. Phys.* **1972**, *56*, 2257−2261.
(54) Francl, M. M.; Pietro, W. J.; Hehre, W. J.; Binkley, J. S.; Gordon, M. S.; DeFrees, D. J.; Pople, J. A. *J. Chem. Phys.* **1982**, *77*, 3654−3665.
(55) Gusev, D. G. *Organometallics* **2013**, *32*, 4239−4243.
(56) Marenich, A. V.; Cramer, C. J.; Truhlar, D. G. *J. Phys. Chem. B* **2009**, *113*, 6378−6396.
(57) Weigend, F. *Phys. Chem. Chem. Phys.* **2006**, *8*, 1057−1065.
(58) Weigend, F.; Ahlrichs, R. *Phys. Chem. Chem. Phys.* **2005**, *7*, 3297−3305.
(59) Metz, B.; Stoll, H.; Dolg, M. *J. Chem. Phys.* **2000**, *113*, 2563−2569.
(60) Ribeiro, R. F.; Marenich, A. V.; Cramer, C. J.; Truhlar, D. G. *J. Phys. Chem. B* **2011**, *115*, 14556−14562.
(61) Wiberg, K. B. *Tetrahedron* **1968**, *24*, 1083−1096.
(62) Reed, A. E.; Curtiss, L. A.; Weinhold, F. *Chem. Rev.* **1988**, *88*, 899−926.
(63) Weinhold, F. *J. Comput. Chem.* **2012**, *33*, 2363−2379.
(64) Huang, D.; Makhlynets, O. V.; Tan, L. L.; Lee, S. C.; Rybak-Akimova, E. V.; Holm, R. H. *Proc. Natl. Acad. Sci. U. S. A.* **2011**, *108*, 1222−1227.
(65) Liang, Y.; Liu, S.; Xia, Y.; Li, Y.; Yu, Z.-X. *Chem. - Eur. J.* **2008**, *14*, 4361−4373.
(66) Chan, W. W.; Lo, S. F.; Zhou, Z.; Yu, W. Y. *J. Am. Chem. Soc.* **2012**, *134*, 13565−13568.
(67) Suzuki, Y.; Sun, B.; Sakata, K.; Yoshino, T.; Matsunaga, S.; Kanai, M. *Angew. Chem., Int. Ed.* **2015**, *54*, 9944−9947.
(68) Li, L.; Brennessel, W. W.; Jones, W. D. *Organometallics* **2009**, *28*, 3492−3500.
(69) Gorelsky, S. I.; Lapointe, D.; Fagnou, K. *J. Am. Chem. Soc.* **2008**, *130*, 10848−10849.
(70) Boutadla, Y.; Davies, D. L.; Macgregor, S. A.; Poblador-Bahamonde, A. I. *Dalton Trans.* **2009**, 5820−5831.
(71) Um, I.-H.; Kim, M.-Y.; Bae, A.-R.; Dust, J. M.; Buncel, E. *J. Org. Chem.* **2015**, *80*, 217−222.
(72) Xia, Y.; Liang, Y.; Chen, Y.; Wang, M.; Jiao, L.; Huang, F.; Liu, S.; Li, Y.; Yu, Z.-X. *J. Am. Chem. Soc.* **2007**, *129*, 3470−3471.
(73) Park, S. H.; Kwak, J.; Shin, K.; Ryu, J.; Park, Y.; Chang, S. *J. Am. Chem. Soc.* **2014**, *136*, 2492−2502.
(74) Xu, X.; Liu, P.; Lesser, A.; Sirois, L. E.; Wender, P. A.; Houk, K. N. *J. Am. Chem. Soc.* **2012**, *134*, 11012−11025.

DOI: 10.1021/acs.joc.6b02962
J. Org. Chem. 2017, 82, 1195−1204